STUDIES ON FATIGUE DAMAGES BASED ON STRAIN
MEASUREMENTS OF A HIGHWAY BRIDGE

By Shugo KATO*, Osamu YOSHIKAWA**, Hiromasa TERADA*** and
Yoshio MATSUMOTO***

The strain behavior at the connection plate between main girder and transverse bracing in
a simply supported composite plate girder is studied in order to find the causes of fatigue
cracks. These cracks occur mainly at the upper end of stiffening plates and rib plates for
connection, and propagate into the web plates of main girders. The strains measured in
field tests are analyzed and fatigue investigations are carried out using Miner's Law. As
the result, it is clear that cracks are initiated by cyclic high stress due to unequal
deflection of main girders and deformation of slab plate at the front toe of fillet welds
between flange plate and stiffener or rib.

1. INTRODUCTION

The highway bridges in the urban area of Japan have been constructed for 20 years.

At present, the steel highway bridges are subjected to the heavier traffic loads and the higher traffic volume due to economic growth than those expected at the time of construction.

The specifications of highway bridges in those days were Steel Highway Bridge Design Specification in 1964 and its Supplement in 1967. The reinforced concrete slab and the transverse members designed by these specifications were deficient in rigidity compared with those by the present specification. As a result, there are many bridge slabs that need repaires and rehabilitations to support today's vehicle loads.

Recently it has been reported that numerous steel bridges have experienced fatigue damages as a result of cyclic stresses induced by their distortion[1].

Fatigue cracks have formed at the end of vertical stiffeners at sway bracings and at the end of transverse cross beam connection plates in very common types of plate girder bridges, whatever it is composite or non-composite and simple or continuous.

Unfortunately, designers have not considered the sort of behavior that caused this cracking. Cracks propagate to the web plates of main girder after penetrating across the stiffener or connection plate, but the rate of propagating speed is not so fast and cracks do not transfer into flange plates of main girders, which are under compressive stresses. Therefore, these cracks do not result in the immediate failure of entire bridges. However it is desirable to know the mechanism of these crack initiation and its propagation and to prepare the plan of repair and rehabilitation, because there are many same types of bridges and it is

---

  * Member of JSCE, Hanshin Expressway Public Corporation (Kita-kyutaro, Higashi-ku, Osaka 542)
 ** Member of JSCE, Hanshin Expressway Public Corporation (Kita-kagaya, Suminoe, Osaka 559)
*** Member of JSCE, Yokogawa Bridge Works Co., Ltd. (Shinminato, Chiba 260)

hard to repair after crack length becomes large.

This paper discusses the strain behavior measured at the cracks in the field loading tests on a standard type of composite plate girder bridge of Hanshin Express Way and examines the fatigue cracking.

2. FIELD TESTS

To identify the behavior of the structure, strain measurements were taken in the simple composite plate girder bridge shown in Fig. 1, which was brought into use in 1960.

This bridge with span 26.9 m consists of five main girders, one cross beam at span center and four sway bracings arrranged at 4.5 m spacing. These sway bracings are not considered to support the live load. Therefore, this bridge is a grid-type structure of five main girders and one cross beam, and its grid bending rigidity is $Z=7$.

Ten years after construction, cracks developed on the floor slab of 18 cm thick and they have been continuously reinforced by bonding steel plate on its lower surface, where the steel plate thickness was 4.5 mm. Fig. 2 shows the structural details and cracks that have developed at the ends of stiffeners at sway bracing and of cross beam connection plates. These cracks have developed at the toe of fillet welds and/or at the center of scallops, and propagated along the weld beads.

(1) Installation

To recognize the load transfer mechanism, strain gages are attached on the main girders, cross beam, sway bracings, and the ends of stiffeners and connection plates. Moreover, displacement is measured on the slab and main girders. These are installed on the down-line side shown in Fig. 1.

(2) Loading and measuring method

Tests were done under three types of loading : (a) static loading test using a 20-ton truck, (b) running test using the same truck with its speed of 40 and 60 km/h, (c) strain response test under actual traffic. Used truck for tests (a) and (b) is shown in Fig. 3 and these tests were carried out at midnight under controlled traffic.

Tests (c) were carried out in the typical traffic period for two hours, three times a day which were early morning, evening and midnight.

Measurements were done three times each for the following three traffic conditions ; two-way traffic and
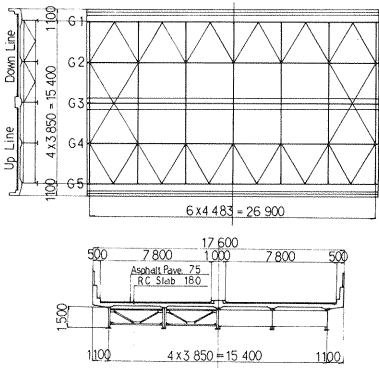

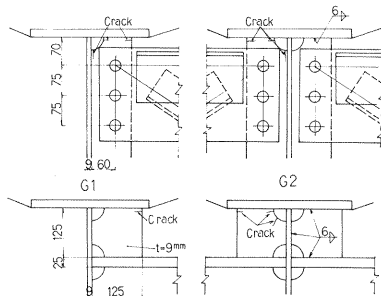
Fig. 1   Test bridge.

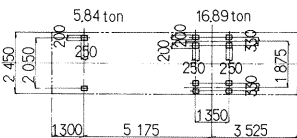Fig. 2   Details and crack pattern.
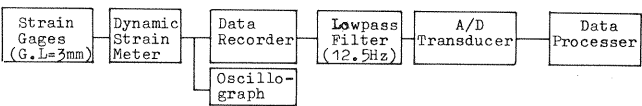

Fig. 3   Loading truck.

Fig. 4   Measurement block diagram.

one-way traffic on either down-line only or up-line only.

The flow of measurement, adjustment and recording is shown in **Fig. 4.**

3. TEST RESULTS AND CONSIDERATION

(1) Results of static and running tests

a) Strain behavior in cross beam

Measured strain distributions are shown in **Fig. 5**, where the center of rear axles of the loading truck is set on the cross beam. The calculated ones are obtained on the basis of the influence line of the grid-structure system. Usually, the bending moment of cross beam at the exterior girder Gl is assumed to be zero in the calculation, because the torsional rigidity of a plate girder is very small. It is however obvious from **Fig. 5** that the bending moment actually occurs at that point in spite of the assumption in the calculation. Moreover, it seems that the normal force exists together with bending moment.

The mechanism of this behavior can be considered as follows.

As the structure is loaded, main girders deform differently at the position where the cross beam is attached as shown in **Fig. 6** (a), resulting in bending moment and shearing force in a cross beam.

At the same time, the distortion of a slab rotates the upper flange of main girders as in **Fig. 6** (b). Then the cross beam resists to these behavior, and normal force, bending moment and shearing force emerge at the end of the cross beam.

Then under the assumption of the behavior of main girders, the calculated stress distibutions become as shown in **Fig. 7**. Although there are some discrepancy between calculated and measured stress distributions, they show the same tendency. The influence of slab deformation therefore cannot be negligible contrary to the assumption in the previous calculation.

b) Strain in sway bracings

Fig. 8 (a) shows the measured member forces of the sway bracing near the center of the span.
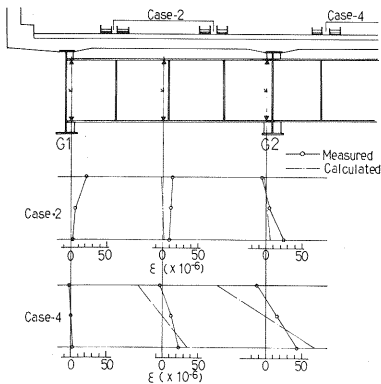
The values in the parenthesis of **Fig. 8** (a) are

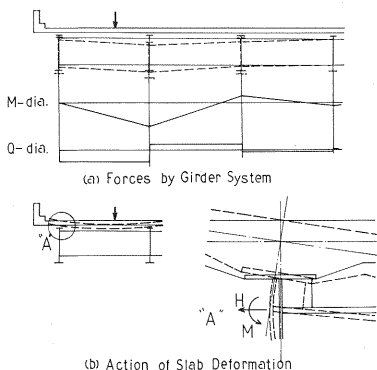Fig. 5　Measured strain of cross beam.

Fig. 6　Improved assumption of behavior of cross beam.
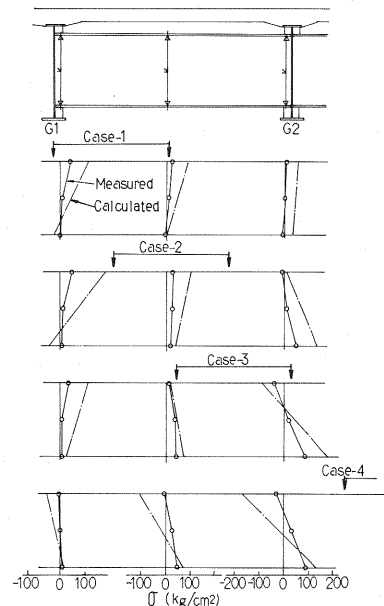
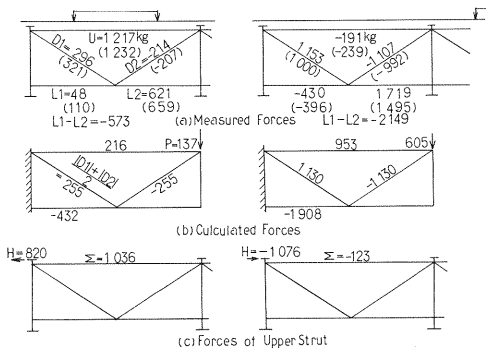Fig. 7　Improved stresses of cross beam.
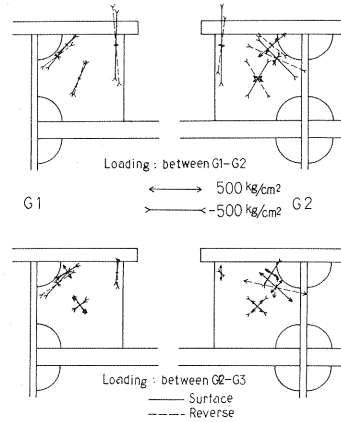
Fig. 8   Member forces of sway bracing.

Fig. 9   Principal stresses in rib plate.

those of the sway bracing adjacent to the support.

Both are under direct loading on each sway bracing. These results clearly imply that the member forces are quite similar in two sway bracings and that the amount of the diflection of main girders does not have any influence on the member forces. Moreover, the actual member force of the upper strut is larger than the calculated one, and do not balance with those of other members as a truss.

Here, assuming a sway bracing to be a cantilever truss, following analysis is done. At first, the measured forces in the diagonal members are presumed to show the behavior as a truss because they agree with each other. Then the load to act at the end of a cantilever truss is calculated using the force in the diagonal member, so the forces to act in the upper and lower struts are obtained as shown in Fig. 8 (b). The horizontal forces H in Fig. 8 (c) are the effect of horizontal deformation due to the distortion of a slab shown in Fig. 6 (b). The sum of the force in the upper strut is similar to the measured force, so the assumption may be correct.

These results imply that the force acting on the upper strut is composed of the forces due to not only the differential amount of girder displacement but also the horizontal deformation of the upper flange resulted from the deflection of the slab. As to the forces of lower struts, the difference between L1 and L 2 in measured forces nearly equal the calculated one as shown in Fig. 8 (a), (b). This may be because the compressive force, which should act on the lower strut L 1, is imposed on the strut L 2 due to the lower out-of-plane rigidity of the exterior girder G 1.

c)   Measurement at cross beam connection plates (rib plates)

Fig. 9 shows the measured principal stresses of rib plates. The broken lines in Fig. 9 are of the back of plates.

The compressive stresses are dominant on both sides of rib plates at the exterior girder G 1, and the tensile stresses which might cause fatigue cracks are not observed. Generally higher stresses occur at the tip and center of scallops, that correspond to the crack positions.

The stresses of the rib plate in the main girder G 2 are sensitive to the loading positions, that is, the compressive stresses emerged in the case of loading between G 1-G 2 are altered to the tensile stresses when the load is applied between G 2-G 3. The rib plate at the main girder G 2 is therefore always under the alternate stress condition.

Moreover, since the relative deflections induced by these two different loadings seemed to be equal, a main factor of the alternate stresses is slab deflection. Since the measuring point at the tip was at the distance of 7 mm from the weld toe and edge of scallops, it is easily expected that the higher alternate stresses might act at the positions where cracks are initiated.

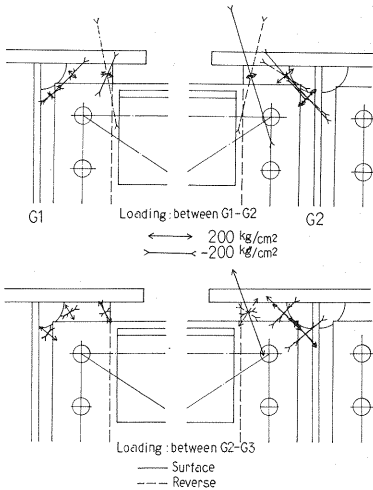d)   Measurement at stiffeners for sway bracings

Fig. 10   Principal stresses in stiffeners.

Fig. 10 shows the principal stresses at stiffeners on static loading test. The tendency of measured stresses are similar to those at rib plates, except that the stresses in the stiffener at the girder G 1 is alternating with loading cases, and that the magnitude and direction of the principal stresses change from the front side to the back side.

This would result from the out-of-plane bending by the structural eccentricity of stiffeners and guesset plates connecting sway bracing members. The stresses in the stiffener at the main girder G 2 show higher levels than those in the stiffener at G 1. This fact agree with the frequency of crack occurence.

e)   Strain behavior in running test

Dynamic strain measurements were done at the some gage points, where larger strains were obtained in the static loading test.

Typical strain responses are shown in Fig. 11 and 12, where the running speed of the truck was 40 km/h.

The strain responses at the rib plate show only one mode, which indicates the cross beam to act as a part of main structure system.

As compared with the case of loading between G 2–G 3, the strain response in the case of loading between G 1–G 2 shows the complex shape and the effect of direct loading can be readily observed.

The strains of the rib plate at G 1 is compression on both loading cases but that at G 2 is alternated by each loading case.

Furthermore, the magnitude of strains at the tip and center of a scallop is alternative in accordance with the case of loading. The strain responses in stiffeners differ a little with those in rib plates shown in Fig. 12. The responses at the loading between G 1–G 2 are sensitive to the individual axle loads. The stiffener in G 1 is always suffered the large out-of-plane bending, which consists with the result of static test.

In the loading between G 2–G 3, it is relatively smooth curves because of the relief of slab action resulting from the indirect loading.

(2)   Strain behavior under actual traffic (random loading)

The strains measured at early morning (6 : 00–8 : 00), which are larger than those at another time zones, are shown in Table 1 with the results of static and running tests. As the results of static test are similar to the running test results, the dynamic increment of strains cannot be observed. It seemed that the road surface was relatively under good condition and the speed of the truck was slow of 40 km/h and 60 km/h.
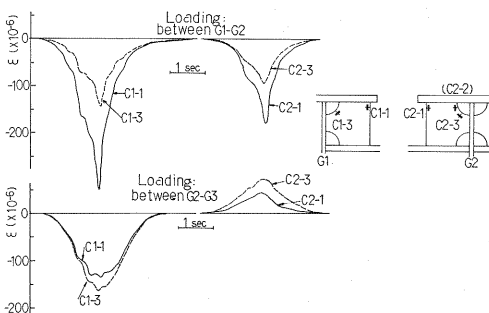

Fig. 11   Strain behaviors of rib plates.

Fig. 12   Strain behaviors of stiffeners.

Table 1　Strain difference at each test.

(a) Cross Beam Rib　　　　　　　　　(×10⁻⁶)

	Gage	Strain	Static	Dynamic	Random
G1	C1-1	ε_{max}		13	70
		ε_{min}	-310	-306	-520
		$\varepsilon_{max}-\varepsilon_{min}$	310	319	590
	C1-3	ε_{max}		20	30
		ε_{min}	-184	-169	-320
		$\varepsilon_{max}-\varepsilon_{min}$	184	189	350
G2	C2-1	ε_{max}	73	75	80
		ε_{min}	-348	-354	-530
		$\varepsilon_{max}-\varepsilon_{min}$	421	429	610
	C2-3	ε_{max}	183	162	210
		ε_{min}	-223	-202	-440
		$\varepsilon_{max}-\varepsilon_{min}$	406	364	650

(b) Sway Bracing Stiffener　　　　　　　(×10⁻⁶)

	Gage	Side	Strain	Static	Dynamic	Random
G1	S1-1	A	ε_{max}	39	42	70
			ε_{min}	-61	-82	-200
			$\varepsilon_{max}-\varepsilon_{min}$	100	124	270
		B	ε_{max}		5	20
			ε_{min}	-225	-212	-450
			$\varepsilon_{max}-\varepsilon_{min}$	225	217	470
G2	S2-1	A	ε_{max}	171	112	150
			ε_{min}	-273	-238	-420
			$\varepsilon_{max}-\varepsilon_{min}$	444	350	570
		B	ε_{max}	42	66	80
			ε_{min}	-241	-210	-460
			$\varepsilon_{max}-\varepsilon_{min}$	283	276	540

On the contrary, the strains under random loading are 1.7~2.7 times as much as the results of static and running tests. Since the plural vehicles might load on each lane, larger strain responses were expected. But the measured strains are more than predicted ones in the calculations. Therefore, the traffic of vehicles over 20 ton in total weight are supposed.

The maximum strain range is 650×10^{-6} at the position of gage C 2-3, which is 1 365 kg/cm² in term of stress. As the position of gage is at the distance of 7 mm from the weld toe and at the same time the dead load stresses are working, the stress at the weld toe is evident to be significant magnitude. But it is difficult to explain the crack initiation and development because compressive streses are dominant at any points. While the existence of the high tensile residual stresses in fabrication therefore must be considered, they are influenced by the fablication method and welding procedure. So the measurement of residual stresses under various fabricating conditions may be needed in future.

(3)　Fatigue analysis

a)　Strain range-cycle relationship

Fig. 13 shows an example of strain response, which is of the gage S 2-1 A at the stiffener in Table 1.

From the response curves as this, the strain range-cycle relationships are obtained at every 10×10^{-6} strain based on the rainflow method. The relationships show straight lines for each response as shown in Fig. 14, where the vertical axis shows the strain range $(\sigma_{max}-\sigma_{min})$ and the horizontal axis the accumulate cycles taking the log.

b)　Estimation of strain range-cycle in the service life of 14 years

The major strains are dominated by the loading on the down-line, and the influence of the loading on up-line is very small because the measuring positions are settled in the side of down-line.

Therefore, the results under the traffic of two lines and down-line are assumed to be equivalent and are treated as the data of four hours for each measuring time.

The estimation of the strain range-cycle in the service life of 14 years are carried out on the following assumptions.

①　The traffic in a day is classified to three patterns of early morning-evening (6：00-17:00), evening-midnight (17：00-24:00), and midnight-early morning (24：00-6：00) according to the traffic

Fig. 13　Strain response as a function of time.

Fig. 14　Strain range spectrum.

volume and its composition. The measuring time periods of each two hour are supposed to represent the portion of such pattern.

②　The traffic composition is assumed to be constant ever since the bridge has been constructed, and also the measured cycles at each time period can be proportionally extended to the total traffic volume in 14 years.

③　But the magnitude of traffic loads must be limited to a certain extent. Provided that the traffic volume in measuring time periods is extended proportionally to whole service life of 14 years, it may result in extremely high strain estimation. Therefore, it is considered in order to put the unsuitable high strains out of the way that the some constant traffic volume (one volume unit) must be settled and this unit affects repeatedly.

The volume unit is supposed as fifty thousand vehicles based on the other data about the intensity of axle loads[2], in which one truck of the axle load 35-ton is contained. Where, the axle load is obtained the tandem axle loads to convert into one equivalent load as shown in **Fig. 15**.

Based on the above mentioned assumptions, strain range-cycle relationships in whole service life are calculated using the measured strain range-cycle relationship as following equation.

$$\binom{\text{Strain-cycle relation}}{\text{at each time period in service life}} = \binom{\text{Measured S-N relation}}{\text{at each time period}} \times \frac{(\text{Traffic volume in each patten in one unit})}{(\text{Traffic volume in measured time period})}$$
$$\times \binom{\text{Unit numbers}}{\text{in service life}} \cdots\cdots\cdots\cdots\cdots\cdots\cdots\cdots\cdots (1)$$

The total traffic volume in the service life on down-line is 167 500 000 which is gained by the investigation data on traffic volume a day. Therefore, the unit numbers in the service life in eq. (1) are

167 500 000/50 000＝3 400

The example of calculated strain range-cycle relationship based on the procedure are shown in **Fig. 16** on the weld toe of a stiffener. Also the maximum strain ranges calculated are listed in **Table 2**.

The strains in static loading in **Table 2** show the calculated ones by loading the maximum load onto the influence lines obtained from the static test. It is apparent from **Table 2** that the maximum strains on the strain range-cycle relationship agree with the calculated static strains, and the assumption of this procedure may be nearly appropriate.
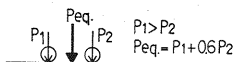

Fig. 15　Assumption of equivalent load.

Table 2　Estimated strains by loading tests.

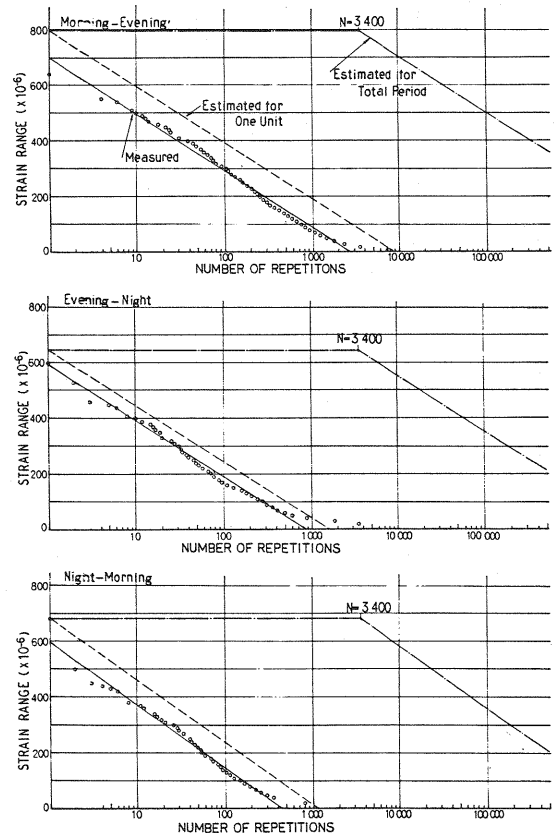| Measured Point			Random Loading (A)			Static Loading (B)	(A)max / (B)
			Morning –Evening	Evening –Night	Night –Morning		
Sway Bracing	G1	S1-1A	293	219	242	300	0.98
		S1-1B	643	448	500	618	1.04
	G2	S2-1A	796	649	685	1 150	0.69
		S2-1B	763	497	620	733	1.04
Cross Beam	G1	C1-1	807	676	694	907	0.89
		C1-3	446	363	402	508	0.88
	G2	C2-1	928	772	795	1 163	0.80
		C2-2	272	197	242	321	0.85
		C2-3	792	610	703	1 051	0.75

Fig. 16　Estimation of strain-frequency.

c) Determination of fatigue damage

The fatigue damage is determined from Miner's linear damage relationship of equation (2), in which stresses are considered as full stress range $S=(\sigma_{max}-\sigma_{min})$.

$$F_d=\Sigma\frac{n_i}{N_i}=\left(\frac{n_1}{N_1}+\frac{n_2}{N_2}+\cdots\cdots+\frac{n_n}{N_n}\right)\cdots\cdots\cdots\cdots\cdots\cdots\cdots\cdots\cdots\cdots\cdots\cdots\cdots\cdots (2)$$

Where F_d=fatigue damage ratio, n_i=frequency of strain range S_i and N_i=number of repetitions to failure in strain range S_i.

Frequency n_i in eq. (2) is given by eq. (3) from the strain range-cycle life relationship.

$$n_i=(n_i'-n_{i+1}')\times N'\cdots\cdots\cdots\cdots\cdots\cdots\cdots\cdots\cdots\cdots\cdots\cdots\cdots\cdots\cdots\cdots\cdots\cdots\cdots\cdots (3)$$

where n_i', n_{i+1}'=frequency of applied repetitions at strain range in a unit, N'=numbers of unit in the service life.

In order to determine the fatigue damage for each structural datail, design $\sigma_\gamma-N$ curves of Japan Steel Railway Bridge Standard (JNR for short)[3], Fatigue Design Specifications by Society of Steel Construction of Japan (JSSC)[4] and British Standard BS 5 400, part 10 (BS)[5] are applied. The category is assumed as a non-load-carrying fillet weld to the weld toe and as a holed plate to the scallop. Design $\sigma_\gamma-N$ curves of each specification are shown in Fig. 17, 18.
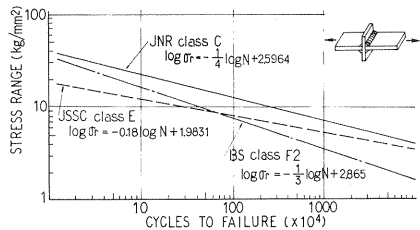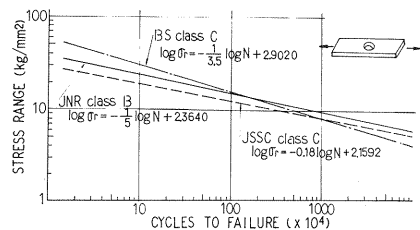

Fig. 17 Basic fatigue strength for fillet weld.

Fig. 18 Basic fatigue strength for plate with a hole.

Here, the basic fatigue strength on the holed plate differs from JNR and JSSC to BS, that is, the basic fatigue strength is provided as the nominal stress σ_0 in JNR and JSSC as against the edge stress $\sigma_c=K\sigma_0$ in BS, where the stress concentration factor at the edge of a hole is $K=2.4$. Measured stresses are compensated therefore for following alternations, respectively, and then compared to each design $\sigma_\gamma-N$ curve.

JNR, JSSC : $\sigma_0=\sigma_M/K_M$
BS　　　 : $\sigma_0=\sigma_M\cdot K/K_M$

where σ_M=measured stress $(=\varepsilon\times E, \ E=2.1\times10^4 \ kg/mm^2)$, K_M=stress concentration factor at measured position, K=stress concentration factor 2.4 at the edge of a hole in BS.

d) Evaluation of Miner's summation

Using eq. (2) and design $\sigma_\gamma-N$ curves shown in Fig. 17, 18, Miner's summations are estimated. The strain step on the calculation is every 10×10^{-6}. In the calculation on BS, the number of repetitions in stress range σ_0, which is smaller than σ_0 at $N=10^7$, is reduced in proportion to $(\sigma_\gamma/\sigma_0)^2$ based on the specification. The results are shown in Table 3.

They differ considerably according to the difference of the design $\sigma_\gamma-N$ curves in each specification. But, since the summations at the edge of stiffeners in G 2 are $F_d\gg1$ except by JNR, the fatigue damages come to the expectations. It is applicable to the weld toes

Table 3 Results of the culculation of F_d

Point		BS 5400 Each	BS 5400 Total	JSSC Each	JSSC Total	JNR Each	JNR Total
S1-1A	I	0.047		0.007		0.004	
	II	0.006	0.062	0.001	0.009	0.001	0.006
	III	0.0009		0.001		0.001	
S1-1B	I	0.925		0.638		0.115	
	II	0.104	1.175	0.045	0.764	0.011	0.143
	III	0.146		0.081		0.017	
S2-1A	I	2.129		2.327		0.308	
	II	0.389	2.896	0.378	3.160	0.055	0.421
	III	0.378		0.455		0.058	
S2-1B	I	1.331		1.468		0.194	
	II	0.144	1.704	0.079	1.778	0.017	0.244
	III	0.229		0.231		0.033	
C1-1	I	2.216		2.505		0.325	
	II	0.380	2.998	0.434	3.428	0.057	0.444
	III	0.402		0.489		0.062	
C2-1	I	2.717		4.683		0.465	
	II	0.759	4.064	1.072	6.785	0.122	0.690
	III	0.588		1.030		0.103	
C2-2	I	0.031		0.004		0.003	
	II	0.004	0.044	0	0.005	0	0.004
	III	0.009		0.001		0.001	
C1-3	I	0.020		0.0002		0.0002	
	II	0.003	0.031	0	0.0002	0	0.0002
	III	0.005		0		0	
C2-3	I	0.477		0.011		0.006	
	II	0.074	0.653	0.001	0.015	0.001	0.008
	III	0.102		0.003		0.001	

I : Morning-Evening　　II : Evening-Night
III : Night-Morning

at the cross beam ribs in the main girder G 1 and G 2, too. It is however troublesome to explain the fatigue damage at the center of scallops in G 1 and G 2, because the maximum summation is $F_a=0.653$ by BS. For these positions, the high tensile residual stresses due to the restriction by horizontal and vertical welds and the existence of notches due to flame-cut must be taken into consideration.

Moreover, the design $\sigma_\gamma - N$ curves for the datails as taken up a problem are needed to be prepared in future.

e) Estimation of required fatigue strength

Here, the required fatigue strength in order to prevent the crack initiation is discussed.

Provided that the service life of highway bridges is 50 years and the volume of traffic a day is 46 000 vehicles which is at saturated state, the following repetition numbers Nd of a unit in the service life are obtained.

$N_d=46\,000\times365$ days $\times50$ years$/50\,000=16\,790$ units

The allowable fatigue damage Da per a unit is

$D_a=1/16\,790=5.956\times10^{-5}$

The fatigue damage on a unit for the positions S 2-1 A and C 2-1 on the basic fatigue strength of JNR are as follows, where the design curves (inverse slope of log σ_γ/logN curve is 4) and the Miner's summation in JNR are used.

S 2-1 A : $D_{j,\,s}\,2=0.421/3\,400=1.2376\times10^{-4}$

C 2-1 : $D_{j,\,c}\,2=0.690/3\,400=2.0282\times10^{-4}$

Weld toes require the following fatigue life times to satisfy the design qualifications.

S 2-1 A : $D_j/D_a=1.2376\times10^{-4}/5.956\times10^{-5}=2.08$ times

C 2-1 : $D_j/D_a=2.0282\times10^{-4}/5.956\times10^{-5}=3.41$ times

From these values and $\sigma_\gamma - N$ relationship $\sigma^m=K$, in which $m=$inverse slope 4 and $K=$constant, the modified $\sigma_\gamma - N$ curves are

for the weld toe of stiffeners : log $\sigma_\gamma=-1/4$ log N$+2.67585$ ·· (4)

for the weld toe of ribs : log $\sigma_\gamma=-1/4$ log N$+2.72947$ ·· (5)

The required fatigue strength at the weld toes at two million repetitions results in $\sigma_{200}=12.61$ kg/mm^2 for stiffeners and $\sigma_{200}=14.26$ kg/mm^2 for cross beam ribs. These values correspond to the strength between class B ($\sigma_{f0}=12.7$ kg/mm^2) and class A ($\sigma_{f0}=15.3$ kg/mm^2) in the category of JNR. It is hard to increase the fatigue strength with the retrofit methods such as grinding, peening or arc remelt. The reinforcement in tructural details may be needed in order to prevent the excess stresses initiating cracks.

4. SUMMARY

For the fatigue cracking at the weld toes and scallops in stiffeners and cross beam ribs on composite plate girder bridges, the measurements and the fatigue analysis in order to try to find the causes have been taken.

The results are as follows.

(1) Though the cross beams usually are assumed to be hinge connection with the exterior main girder, measurements shows the actions of bending moment and normal force at the position. This is because the cross beam resists to the out-of-plane displacement of the main girders caused by the deformation of a concrete slab under live loads.

(2) It is applicable to sway bracings, too. But, this effect have not been considered in usual design procedure.

(3) The rib plates for cross beams and the vertical stiffeners for sway bracings showed the complicated strain behaviors resulting from the deformation of a slab and the effect of the live loads. Since the principal stresses measured at the positions of fatigue cracking were mainly compression, it would be hard to explain the occurrence of fatigue cracks. To take account of the initial imperfections such as tensile

residual stresses and deformations at fabrication might be needed.

(4) Since the large out-of-plane bending was noticed on stiffeners, the influence of the structural eccentricity between a stiffener and a gusset plate of sway bracing might be supposed. Considering the crack appearance such that the cracks on stiffeners initiate at the reverse side of gusset plates, it is to be desired to get rid of the structural eccentricity in the connection details.

(5) Comparing the strains measured in static loading and running test using a 20-ton truck with those in actual traffic, the latter showed two times the former.

The heavy traffic over the design load of 20-ton was supposed therefore.

(6) The estimation of strain history in whole service life was made using the measured strain spectra at typical three time periods and the traffic volume data in their periods and in the service life. As a result, the maximum strain range at weld toes and at the center of scallops of a cross beam rib were 900×10^{-6} and 800×10^{-6}, respectively. Also, it at weld toe of a stiffener was 800×10^{-6}. These excess strain ranges could lead to the fatigue cracks.

(7) On the other hand, the estimated strain ranges, which are obtained the assumed maximum vehicle load of total weight of 58.9-ton to load on the influence lines based on the static test result, are similar to those in actual loadings. The traffic of heavy vehicles corresponding to about three times the design load were supposed therefore and may cause the above mentioned high strain ranges.

(8) Using the design $\sigma_\gamma - N$ curves in JNR, JSSC and BS 5 400, the estimations about fatigue damage are taken based on Miner's linear damage relationship. The results of Miner's summation show the large values such as $F_d > 1$ at the weld toes of a cross beam rib and a stiffener, and fatigue damages are affirmed even if the results vary slightly according to the difference of curves in each specification.

(9) Assuming that the service life is 50 years, the required fatigue strength are calculated for weld toes. The required strength are $\sigma_{200} = 12.6$ kg/mm^2 for the weld toe at a stiffener and $\sigma_{200} = 14.3$ kg/mm^2 at a cross beam rib, where $\sigma_{200} =$ design fatigue stress range at two million repetitions.

(10) It is difficult to get these design fatigue strength with such retrofit methods as grinding and the increment of fillet weld size. The improvement and reinforcing in structural details are necessary to prevent the occurrence of fatigue cracks.

5. ACKNOWLEDGEMENT

REFERENCES

1) Nishikawa, K. : The Fatigue Problem and Repair Rehabilitation of Highway Bridges, The Bridge and Foundation Engineering, Vol. 17, No. 8, 1983 (in Japanese)
2) Hanshin Expressway Public Corporation : Survey of Traffic Loads, 1976
3) JSCE : Specification for Steel Railway Bridges, 1983
4) JSSC : Specification for Fatigue Design by JSSC, JSSC Vol. 10, No. 101, 1975-5 (in Japanese)
5) British Standards Institution : BS 5 400 ; Part 10, Code of practice for fatigue, 1980